EARTH SCIENCES
RESEARCH JOURNAL
Earth Sci. Res. J. Vol. 28, No. 3 (September, 2024): 255 - 263

UNIVERSIDAD NACIONAL DE COLOMBIA

GEOPHYSICS

Subsoil geophysical evaluation using GPR and free software

Hernán Darío Guerrero, Luis Hernán Ochoa
Universidad Nacional de Colombia
Corresponding authors: hdguerreroc@unal.edu.co; lhochoag@unal.edu.co

ABSTRACT

In this work, a geophysical characterization of the subsoil of a civil structure corresponding to the basement of a residential complex in Bogotá, Colombia was carried out, using the GPR technique. We were chosen to establish the affectation caused by weeping willow (Salix Babylonica) trees planted near the retaining wall of the structure's foundation and its parking lot platforms. We acquired GPR profiles all throughout the area of the internal part of the basement and the outer retaining wall part. The pieces of equipment used were SIR 4000 and a HS 350 MHz center frequency antenna. The data presented a good and consistent signal. High resolution subsoil images of up to 3m in depth of the area below the parking lots were generated through the analysis of information derived from the processing and interpretation of the data. All of these were compared with information from geotechnical and topographic studies of the area. The results obtained show that the trees' roots are causing scour due to a drying effect of the subsoil, which caused damage to the slab in the parking lot and on the retaining wall.

Keywords: weeping willow trees; reflection; georadar; GPR; electromagnetic methods; scour; drying effect; subsoil disturbance.

Evaluación geofísica del subsuelo usando GPR y software libre

RESUMEN

En este trabajo, se realizó la evaluación geofísica del subsuelo de una estructura civil correspondiente al sótano de un conjunto residencial en Bogotá, Colombia, utilizando la técnica de GPR. Se seleccionó el área para establecer el impacto causado por árboles de sauce llorón (Salix babylonica) plantados cerca del muro de contención de la cimentación de la estructura y de las plataformas del parqueadero. Se adquirieron perfiles de GPR en toda el área de la parte interna del sótano y en la parte externa del muro de contención. El equipo utilizado fue el SIR 4000 con una antena de frecuencia central de 350 MHz. Los datos presentaron una señal buena y consistente. A través del análisis de la información derivada del procesamiento e interpretación de los datos, se generaron imágenes de alta resolución del subsuelo, alcanzando profundidades de hasta 3 m en el área debajo de los parqueaderos. Toda esta información se comparó con estudios geotécnicos y topográficos de la zona. Los resultados obtenidos muestran que las raíces de los árboles están causando socavación debido a un efecto de desecación del subsuelo, lo cual ha generado daños en la losa del parqueadero y en el muro de contención.

Palabras clave: GPR; georradar; métodos electromagnéticos; reflexión; socavación; efecto de desecación en estructuras; alteración del subsuelo; sauce llorón;

Record
Manuscript received: 15/07/2023
Accepted for publication: 15/12/2024

How to cite item:
Guerrero, H. D., & Ochoa, L. H. (2024). Subsoil geophysical evaluation using GPR and free software. *Earth Sciences Research Journal, 28*(3), 255-263. https://doi.org/10.15446/esrj.v28n3.97305

ISSN 1794-6190 e-ISSN 2339-3459
https://doi.org/10.15446/esrj.v28n3.97305

1. Introduction

Geophysical techniques have been used in different fields such as the mining, oil and gas industry, archaeology, and engineering, with a variety of applications. The use of geophysical techniques has many advantages, such as providing a cost-effective way to investigate conditions at a test site without physical intervention. Geophysical techniques such as ground penetrating radar (GPR), are frequently used because they are able to provide greater spatial resolution at shallow depths by using high frequencies. These provide better resolution than other options like in situ testing. As with all geophysical techniques, each method has limitations and potentially suffers from problems of non-exclusivity. The combined use of different shallow geophysical methods has proven useful in obtaining more robust inversions by adding more information a priori (Besson, 2010).

Several root mappings studies that use GPR have been reported in the literature (Hruska et al., 1999), (Zhang et al., 2019), (Guo et al., 2013), (Moore and Ryder, 2015), (Alani et al., 2018), among many others, where different frequencies from antennas are reported for different depths of investigation, as well as mapping various root systems. In the present study, we adopted a similar methodology, starting with preliminary research to establish the optimal investigation depth. This was followed by the application of standard data processing techniques, yielding images comparable to those reported in previous literature. Typically, high-frequency antennas (greater than 800 MHz) are employed, enabling the detection of root diameters between 10 and 20 cm in shallow subsurface layers (less than one meter). Additionally, GPR is capable of detecting reflections and anomalies associated with deeper root systems. This study aims to assess the impact of tree roots on subsoil conditions, both in proximity to and at a distance from trees, to determine whether root growth is the primary factor contributing to the observed subsurface disturbances.

2. Materials and methods

Investigation site

The data acquisition was carried out in a residential complex located in the northwest of Bogotá - Colombia, which can be seen in the Figure 1.

Damage to the structure

The circulation slab at the south side of the residential complex has multiple damages on its surface. The subsoil below: this area is being affected by something that causes large sags and lifts to occur, breaking the reinforced concrete and causing considerable damage to the structure in question, see Figures 2, 3. The retaining wall also presents damage. This indicates that some elements of the structural system of beams and columns that lead up to it has been affected, with cracks and fissures in these elements.

Trees of interest

There are two lines of trees close to the retaining wall (Figure 4). The tree line that corresponds to the weeping willow line is at a distance of around 2 - 3 m. from the retaining wall. There are fifteen (15) of those trees spread almost evenly along the 150 m of wall, with a height of around 13 - 16 m. on average. The second line of trees is far from the Weeping Willows (more than 3 m.) and corresponds to another tree species of lesser size.

Figure 1. Location Overview of the Study Area. The top image, captured in 2015, shows the site where the geophysical investigation was conducted, located to the south of the building complex. At this time, the trees were still small, and no damage had been reported within the platforms. The yellow rectangle highlights the study area. The bottom image, taken after 2020, shows the same location with significantly larger trees, whose growth coincides with the structural damage reported inside the platforms.

Figure 2. A sag in the plate of approximately 30 cm is observed. The distance between columns is of 5 m. The structural frames were protected with metal trusses for precaution and to prevent aerial beam deflections.

Figure 3. A rise is observed in the parking slab. The thickness of the slab is 15 cm. Several fissures and cracks have been formed.

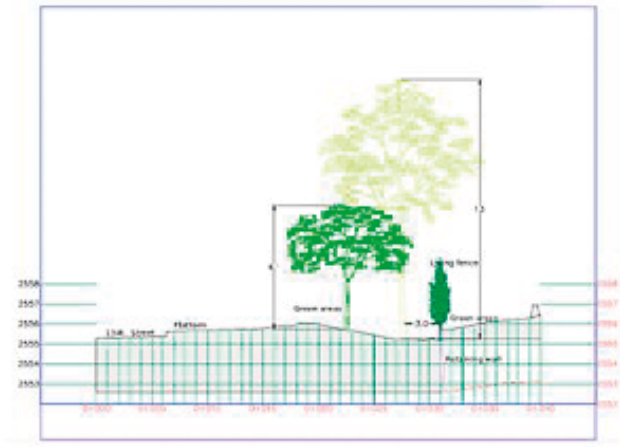

a) Topografic profile

b) GPR Acquisition lines next to the retaining wall

Figure 4. Panoramic view of the zone. Figure a. shows a topographic profile of the section between the wall and the tree line. Figure b. shows the GPR lines acquired outside the wall and inside the basement immediately next to the wall. The difference in height between the profiles taken at (a) and (b) is 2.5 m.

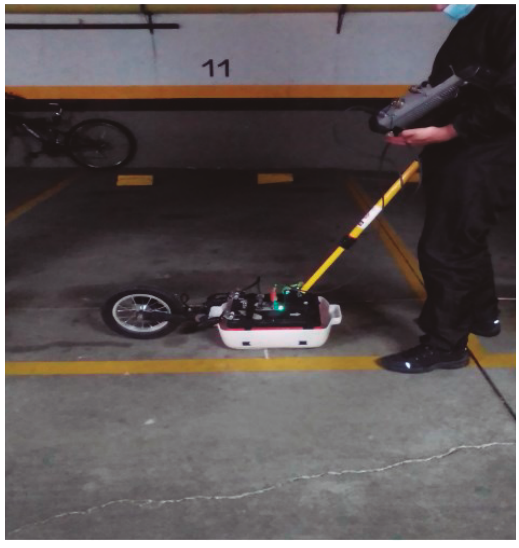

Figure 5. Position of the GSSI 350 HS antenna and the GPR GSSI Sir4000 during the acquisition, on the reflection profile mode.

Equipment

In this work, a GSSI Sir4000™ was used in conjunction with a 350 HS™ antenna (see Figure 5). The SIR 4000 (GSSI, 2017) is GSSI's first high-performance GPR data acquisition system designed to work with both analog and digital antennas. This evolutionary step allows for true versatility and flexibility in supporting a wide range of users in numerous applications. The HS 350 MHz central frequency (GSSI, 2013) is a next-generation digital antenna designed to work seamlessly with the GSSI SIR 4000 control unit and the G1 controller. It is easily configurable to suit any kind of application, including archaeology, geophysics, utility location, and more. GSSI's Hyper Stacking technology considerably improves the depth and performance of data resolution compared to traditional radiated two-stage methods.

3. Ground penetrating radar measurement

The GPR technique is a high-resolution electromagnetic technique that is designed to examine the near subsurface. The main objective is to locate buried objects such as pipes, lithological changes, as well as changes in the structure of the subsoil like defects and cracks in the materials, or differences in humidity due to groundwater content, among others (Finck, 2013).

Ground-penetrating radar (GPR) uses electromagnetic (EM) propagating waves that respond to changes in the electromagnetic properties of the shallow subsurface. The speed of propagation of EM waves, which is the main controlling factor in the generation of reflections, is determined by the relative permittivity contrast between background material and the target (or the contrast between the layers). Relative permittivity (also called the dielectric constant) is defined as the ability of a material to store and allow the passage of EM energy when a field is imposed on the material. This can be measured in the laboratory or in situ (Baker et al., 2007).

GPR operates by transmitting high- frequency electromagnetic pulses on the ground through a transmitting antenna. Pulses are partially reflected and scattered towards the surface from various sub-surfaces of contact between different materials on the ground. That is, those through which there is a contrast in the dielectric constant. This reflected/scattered energy then travels back to the surface, where it is recorded by the receiving antenna. The time it takes for the wave to travel to an interface and return to the surface is called travel time and is used to determine the in-situ propagation speed of the subsurface material.

The velocity (distance/travel time) for an EM wave in the Earth's atmosphere at or near sea level is 0.33 m/ns. Because the relative permittivity of all subsurface materials is greater than the permittivity of air, the velocity of an EM wave in all subsurface materials will be less than the EM propagation velocity in typical air materials between 0.05 and 0.15 m/ns (Daniels et al., 1995). Even though the speed of propagation of an EM wave depends on the relative permittivity of the material, the amplitude and attenuation of a propagation wave depend on the magnetic permeability and electrical conductivity of the material (Baker et al, 2007).

Electrical conductivity also affects the propagation of electromagnetic waves. Materials with high electrical conductivity may attenuate EM signals; Therefore, highly conductive materials will produce poor GPR data and/or reduce penetration depth. The depth of penetration for the investigation is controlled by the radar pulse's frequency, the magnetic permeability (which correlates the magnetic induction with the intensity of the magnetic field), the electrical conductivity, and the permittivity of the ground. The higher the conductivity and permittivity of the soil, the lower the penetration of the electromagnetic pulse. Therefore, the depth of the investigation is inversely related to the frequency. Therefore, the lower the frequency of the signal, the greater the depth of investigation (Daniels et al, 1995, Neal, 2004).

Data acquisition

In the reflection profile mode, the antennas are kept at a constant separation while moving along a profile. The electromagnetic pulses are transmitted over a fixed distance or time interval. The signal is immediately recorded and displayed on a computer screen in the form of GPR profiles, where the vertical axis is the travel time in two directions in nanoseconds (ns) and the horizontal axis is the distance, along with the measured profile. GPR data is collected along with a single profile, or in a grid of profiles to obtain 2D or pseudo-3D information about structures on the ground.

In this work, we acquired GPR data on profiles covering the entire parking platforms area in that zone, which corresponds to the slab with problems in the surface. The acquired profiles in the basement are shown in the Figure 6. The entire acquisition was made with no presence of vehicles.

Considering the structural damage in the parking slab visible on the surface, due to either subsidence, uplift, or fissures, much denser short profiles were made for each affected area, that is, five GPR profiles were taken separated fifty cm from each other (Figure 7).

Other profiles were acquired in zones with no affection by Weeping Willows or other trees, in order to compare their signals.

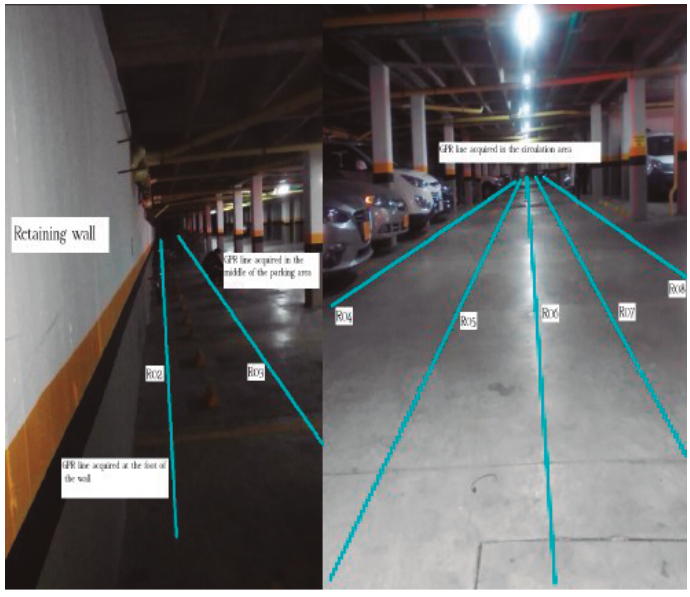

Figure 6. Configuration of the profiles acquired in the parking lots. The lines show the direction and identifier of the profiles of the radargrams.

Figure 7. Location of the short profiles acquired in the basement at parking lots 41 - 42. Trajectories where profiles were taken are outlined in red. Note the great alteration in this parking lot, which shows a fairly large subsidence, as well as many cracks.

Data processing

Jol and Bristow (2003) briefly discuss commonly used data processing procedures. Neal (2004) also discusses the requirements for proper data processing. The next section outlines some of these essential processing steps.

The GPR data was recorded in digital format and was subjected to different mathematical operations that are standard in the basic processing of GPR signals. These involve procedures such as detection of first arrivals, corrections in direct current displacements, time corrections, signal filtering, application of gains, and spatial and frequency filters.

Before the GPR data is ready for interpretation, some processing steps must be applied. The first step is simple data editing to correct errors in the field, as well as inverting profile addresses, merging files, etc. The first regular processing step is "dewow", which removes a long and wavy part of the signal caused by electromagnetic induction.

A time-zero correction was made on the data (see Figure 8). The instrument may not have detected zero time accurately in the field and therefore, it must be reset to ensure correct depths in the profile. Additionally, time-zero drift along the profile can occur due to the temperature difference between the instrument's electronics and the air temperature (Jol et al., 2009). Drift causes reflections to misalign and time-zero must be resampled for all traces, along with the profile (Jol et al., 2009).

By running a bandpass filter over time, the high-frequency electromagnetic noise found in the GPR profile was diminished.

Data processing using RPGR

Today, many commercial software applications that are dedicated 100% to GPR data are available (Huber and Hans, 2018). While many commercial GPR software solutions offer flexible and comprehensive processing capabilities, they often function as "black boxes," where the underlying algorithms and processes are not fully transparent to the user. This lack of visibility makes it difficult to understand exactly how the data is being manipulated. Although these platforms provide advanced features for data visualization, filtering, and interpretation across various applications, the proprietary nature of these tools can limit the user's ability to fully assess or customize the processing steps, which is critical for detailed and accurate analysis. For this reason, we chose to use RGPR, an open-source GPR data processing package that is written in the R language (Ihaka and Gentleman, 1996) because it offers an open source platform with efficient data manipulation tools, strong statistical skills, and tools for graphics and visualization.

RGPR is a ground penetrating radar (GPR) data processing package written in R language (Huber and Hans, 2018). R is a free and open-source high-level programming language for statistical computing. RGPR relies on two main classes for processing and displaying GPR data, as well as for keeping track of processing steps.

The Software in mention was compiled and installed for this work in a Linux Debian 4.9.0-13-AMD64 1 SMP Debian 4.9.228-1 (2020-07-05) x86 64 GNU / Linux operating system which is also of Free use and distribution.

Several scripts in RGPR were written to perform all steps for processing GPR data, in accordance to the literature and in order to get the best results. Below, we show some of these results to evoke how the output is displayed in the software mentioned (Figures 9, 10, 11).

Using the processed GPR data, we conducted an attribute analysis to better interpret subsurface features (Khwanmuang and Udphuay, 2012). For this analysis, we utilized RGPR and OpendTect software to compute various attributes, including instantaneous amplitude, slope, and energy event characteristics. The instantaneous amplitude represents the magnitude of the GPR signal at each point in time, providing insight into the strength of reflections at specific subsurface layers. The slope attribute helps identify the steepness of changes in the signal, useful for detecting anomalies or transitions between layers.

The energy attribute, as defined by Boniger and Tronicke (2010), measures the total energy of the reflected signal by computing the squared sum of the signal values within a specified time range, and then dividing it by the total number of sample times. This attribute is particularly useful for highlighting areas with strong signal reflections, which can indicate changes in material properties or the presence of subsurface structures. Through this comprehensive attribute analysis, we gain a deeper understanding of the subsurface conditions.

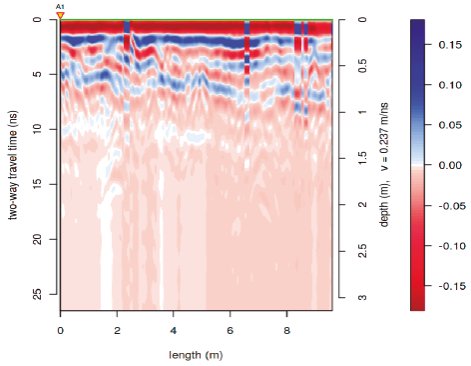

Figure 8. Short profile of radargrams acquired in the basement for a parking lot section. The picture shows time zero correction using RGPR processing.

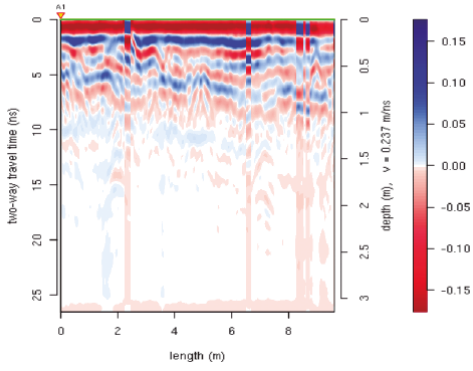

Figure 9. The picture shows low-frequency bands remotion processing using the Dewow procedure in RGPR.

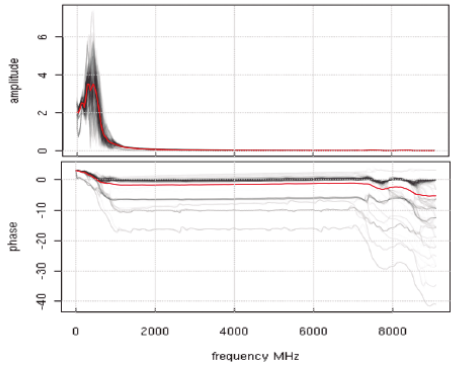

Figure 10. The picture displays the amplitude, frequency and phase in RGPR from the data acquired.

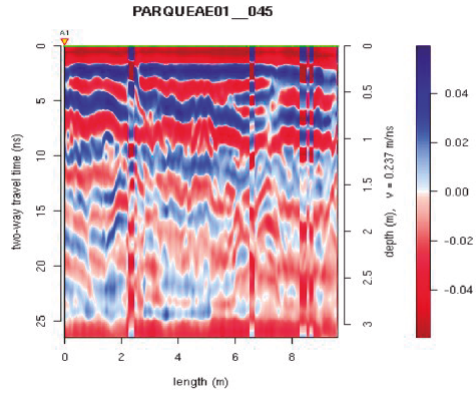

Figure 11. The picture displays the data after the median filter was applied in RGPR.

This attribute enhances areas characterized by strong changes in amplitude. The instantaneous amplitude attribute is determined from the complex trace (Taner et al., 1979) and calculated on a sample by sample basis (White, 1991). It can be used to indicate changes in deposition and contrast between two media. The slope event attribute is the tangent's slope value at a zero crossing of the data-trace (dGB, 2019). It is a useful tool to quantify the quality of the horizons in the data.

Data processing using OpendTect

For better interpretation and analysis of the layers in the subsoil, the processed radargrams were loaded in post-processing software, commonly used for seismic analysis. In this case, we selected OpendTect.

OpendTect is a free, open-source seismic interpretation and post-processing system for visualizing, analyzing, and interpreting 2D, 3D, and 4D seismic data, created by the dGB Earth Sciences™ company (dGB, 2019). It is also widely used for GeoRadar interpretation (Khwanmuang and Udphuay, 2012), (Dujardin et al., 2017), (Tomecka-Suchoń, 2019). OpendTect is released under the GNU Public License (GPLv3 or higher).

For interpretation, OpendTect supports all the tools you expect to find in a seismic interpretation system, including but not limited to the following: 2D, 3D and pre-stack seismic viewers, crossover charts, log viewers Horizon Trackers (Auto, Manual, Grid Tracking, ...) Interpretation of faults Well connection module, Time-depth conversion, 3D bodies Mapping (via GMT). For these reasons, OpendTect is an optimal and very versatile program to visualize the processed data, in addition to having a very high-quality graphical output that is useful for properly identify events and horizons in the GPR data.

Once the data was loaded onto OpendTect, each of the profiles was analyzed in a 2D view and tools for marking and tracking attributes of this program were used. The markings of the events were done by taking small length sections to have a clear and detailed vision, as shown in 12.

It is evident how in certain areas, the reflectors lose their continuity and parts with less dielectric permittivity are noticeable. The variations in the continuity of the reflectors are attributed to changes in the dielectric permittivity of the subsurface materials, which correspond to the presence of different materials or voids. These changes result in signal anomalies, indicating structural disturbances. The red line drawn by the tracker in Figure 12 shows large jumps, showing discontinuities. Some places are not well stratified as can be expected with pavement base material, but they show chaotic behavior instead. These images correspond to areas where a tree behind the wall caused strong effects on the surface.

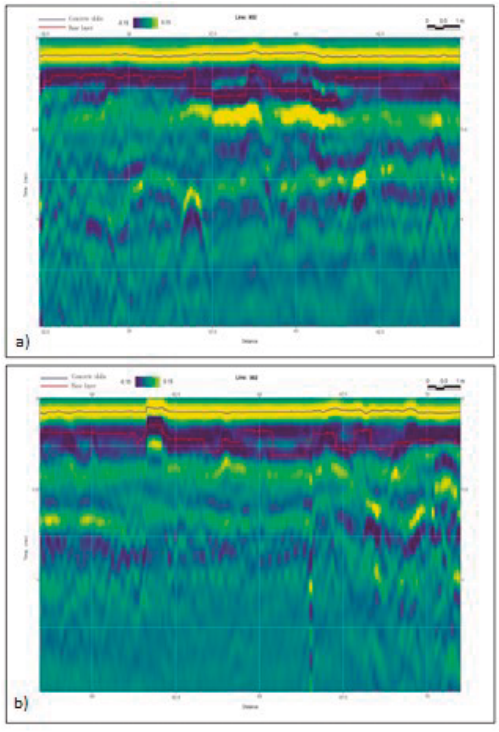

Figure 12. Marking the events using OpendTect.(a) Detail of the interpretation of events on line R002 be-tween meters 32 and 42. (b) Detail of the interpretation of events on line R002 between meters 60 and 70.

4. Interpretation

First, we decided to look for anomalies corresponding to known objects, for example, structural and hydrosanitary elements. We then worked with radargrams throughout time. This is because, through time, the radargrams show a series of signals which can be associated with an anomaly in the layers or reflecting objects. For example, a beam would have an associated signal that is specific to that element's geometry. By following theses kind of patterns, it is easier to identify the structural and hydrosanitary components found in the subsoil under the basement. In terms of depth, all radargrams inside the parking lot had a depth of 3 m. Subsequently, after having identified the anomalies that have obvious explanations, we proceeded to identify those whose origins do not appear on the plans.

Figure 13 shows a close-up of the concordance of GPR events with the structural and plumbing elements of the building, which are fully identified and shown in Figure 14. Similarly, there are more structural and plumbing elements in (Figure 13) that are precisely identified with the interpreted GPR anomalies.

The previous image (Figure 13) displays a small section extracted from a larger radargram. It highlights key elements, including columns (cyan), flooring joists (green), and filters (yellow), along with the corresponding annotations for trees (green). This zoomed-in view facilitates a focused examination of the structural components and their arrangement within the radar data. There is a strong correlation between these anomalies and the structural elements of the building. For a more detailed analysis, please refer to the complete radargram (see Figure 14), from which this section has been extracted.

An analysis of the affectation due to roots outside the retaining wall is shown in Figure 15.

Secondly, having anomalies produced by the structure itself, we proceeded to analyze effects in the subsoil which cannot be related to the structure.

The study on the affectation of the soil due to roots and its detection has bases in the scientific and engineering literature (Kvamme, 2006), (Ramón et al., 2010), (Zhang et al., 2019). These academic studies use GPR calibrated between 500MHz and 1600 MHz to see at shallow depths with high resolution for mapping the roots.

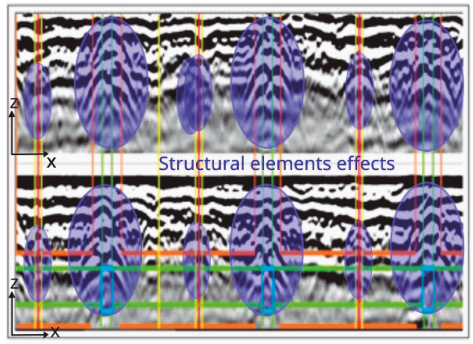

Figure 13. Small section extracted from a larger radargram. This is agreement between detected anomalies and the building's structure. The pictures show two radargrams sections, The anomalies detected in the subsurface have been enclosed in blue ellipses to highlight them. These anomalies correspond to various structural elements, which are marked in different colors for easier identification. The radargrams has beams (green), foundation beams (green), flooring joist (orange), and filters (yellow with red). (x) axis is lateral distance in meters and (z) is depth in nanoseconds.

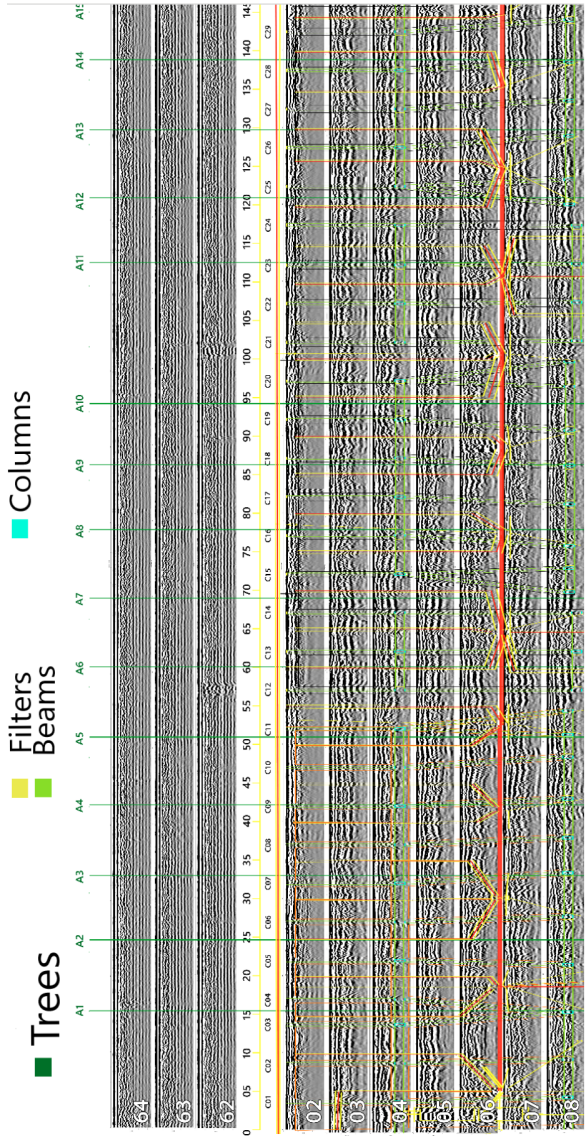

Figure 14. Miniature view of the interpretation of the structural and drainage elements under the subsoil of the parking lot slab

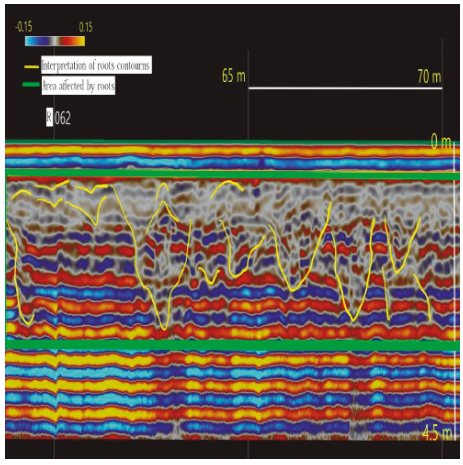

Figure 15. Radargram R62 section taken in the environmental strip at the tree zone. In yellow, we have outlined the contours corresponding to the areas where there is presence from tree roots, very large elements are seen up to 3 m in depth. The disturbance pattern is similar to that of the radar-grams on the other side near the retaining wall. At a greater depth, the signal does not show information.

5. Results

The anomalies detected in the subsoil beneath the parking lot are clearly shown Figures 16, 17, 18, 19 and 20, following the previously described methodology and excluding those attributable to structural and plumbing elements. Each of these figures is marked to highlight the affected areas observed. In this study, the analyses were carried out by dividing each profile into segments of a few meters, as indicated in the aforementioned figures. Additionally, a detailed analysis was conducted for each case where surface damage was evident. For example, Figures 16 to 20 present a three-dimensional visualization of the radargrams, with each radargram positioned according to its respective acquisition location, in Figures 16 and 17, it is clear that the alterations in the subsoil coincide with the proximity of trees to the damaged surface areas. These correlations are documented across all cases, as seen in Figures 18, 19, and 20, where the affected areas show consistent patterns near the trees. This analysis reinforces the interpretation that trees play a key role in the observed damage, a common occurrence when soil desiccation is induced by tree roots. The relationship between root expansion and soil drying often leads to structural issues. Moore and Ryder (2015) highlight that such impacts are significant in assessing the effects of tree roots on their surrounding environment.

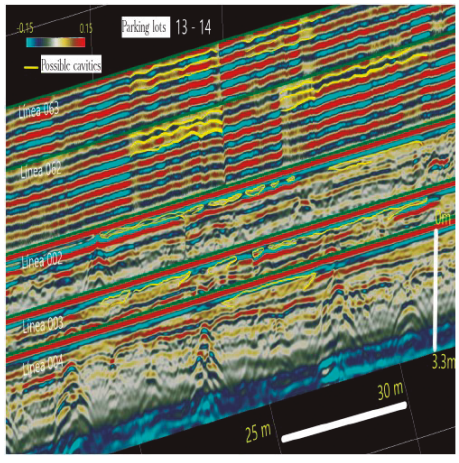

Figure 16. Overview of radargrams analyzed in OpendTect around 20–30 m. The profiles display R063 and R062 (outside the wall) at the top, followed by R02, R03, and R04 (inside the wall). Disturbances in the subsoil highlight the correlation between internal and external areas in sections where Weeping Willows are present.

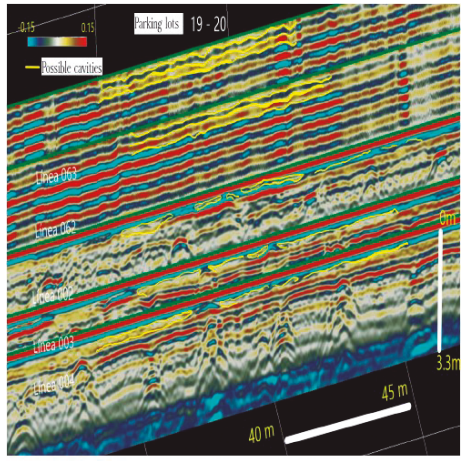

Figure 17. Overview of radargrams analyzed in OpendTect around 35–45 m. The profiles display R063 and R062 (outside the wall) at the top, followed by R02, R03, and R04 (inside the wall). Disturbances in the subsoil highlight the correlation between internal and external areas in sections where Weeping Willows are present.

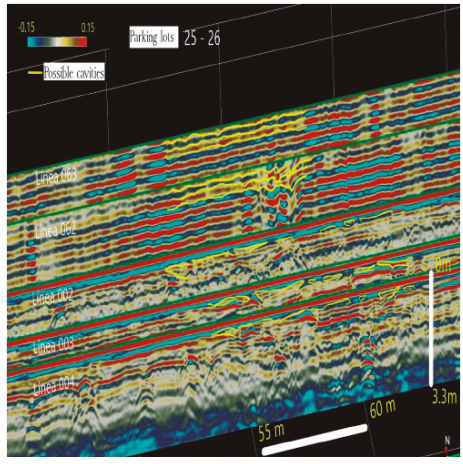

Figure 18. Overview of radargrams analyzed in OpendTect around 50–60 m. The profiles display R063 and R062 (outside the wall) at the top, followed by R02, R03, and R04 (inside the wall). Disturbances in the subsoil highlight the correlation between internal and external areas in sections where Weeping Willows are present.

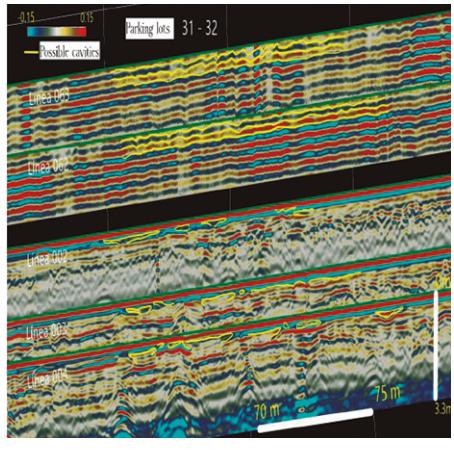

Figure 19. Overview of radargrams analyzed in OpendTect around 65–75 m. The profiles display R063 and R062 (outside the wall) at the top, followed by R02, R03, and R04 (inside the wall). Disturbances in the subsoil highlight the correlation between internal and external areas in sections where Weeping Willows are present.

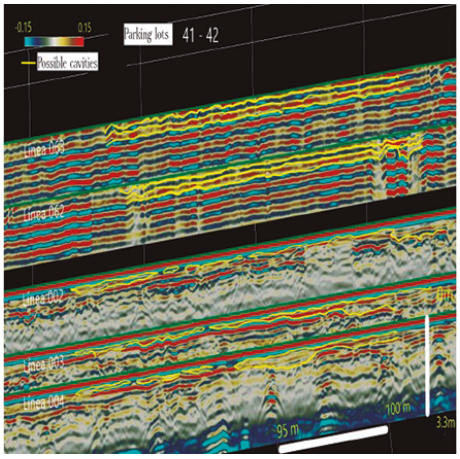

Figure 20. Overview of radargrams analyzed in OpendTect around 90–100 m. The profiles display R063 and R062 (outside the wall) at the top, followed by R02, R03, and R04 (inside the wall). Disturbances in the subsoil highlight the correlation between internal and external areas in sections where Weeping Willows are present.

Radargrams in zones without Weeping Willows

Figures 21 and 22 show examples of a radargram taken in an unaffected soil zone (Radargram 070). This location corresponds to the northern part of the complex. In this place, there is no presence of Weeping Willows.

Figure 21. Radargram R070. No disturbance due to roots is observed. This radargram was obtained in the external northern area of the basement where there is no presence of Weeping Willows.

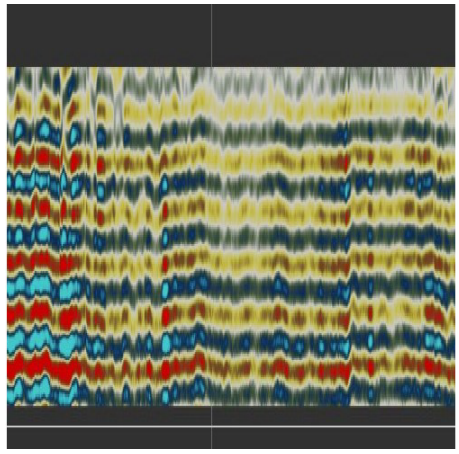

Figure 22. Radargram R070 in OpendTect. The image displays data up to approximately 20 m along the horizontal axis (X), representing distance in meters, while the vertical axis indicates two-way travel time in nanoseconds. There are no disturbances, such as those associated with the roots.

A photographic record obtained from a person associated with the building provides compelling evidence of cavities (Figure 23). These cavities, visible long before the commencement of this study, indicate the onset of surface issues. The presence of a pit at the foot of the retaining wall correlates directly with these surface problems, demonstrating that the initial disturbances were exacerbated by the growth of tree roots in the vicinity. The expansion of these roots can induce soil desiccation, further compromising the structural integrity of the surface (Moore and Ryder, 2015). Moreover, the observed depressions align with the findings in the radargrams, establishing a consistent relationship between the surface manifestations and the anomalies detected in the subsurface. This reinforces the conclusion that the initial surface disturbances, influenced by the growth and desiccation effects of tree roots, significantly contributed to the formation of these cavities, as substantiated by both photographic documentation and radar analysis.

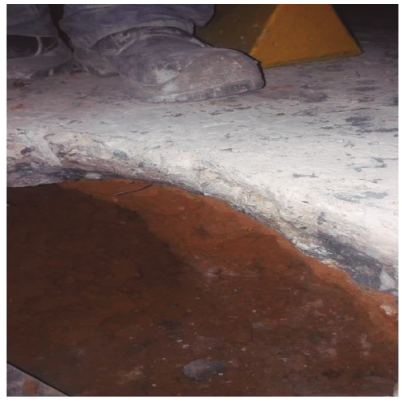

Figure 23. Evidence of scour. It is difficult to estimate the size of the scour, but it is seen to be elongated, which is consistent with what is observed in the GPR records. The exact position of the pit is unknown but is located at the foot of the retaining wall.

Conclusions

Following the established objectives, we successfully carried out geophysical prospecting of the parking area on the south side next to the retaining wall, using ground-penetrating radar. High-resolution images of the first 3 m were obtained under the parking lot, and the following deductions are made from the analysis of the results:

1. The loading, processing, and displaying of acquired GPR data has been done successfully, using free and open-source software tools.

2. It was possible to reconstruct the registered signals and correlate them with the information found in the plans supplied, which correspond to the foundations, as well as structural and plumbing details. A clear correlation is observed between the plans and the data captured by the georadar, as illustrated in Figures 13 and 14. This alignment not only supports the accuracy of the plans but also emphasizes the effectiveness of the georadar in detecting subsurface features. The figures provide a visual representation of this concordance, enhancing the reader's understanding of how the georadar data aligns with the established plans. This specifies that the elements in the drawings do have those sections and they are located according to what is stipulated on them.
3. A reconstruction of the subsoil under the parking lot was conducted. This analysis reveals that the structural platforms in the basement were constructed on a foundation composed of soil for the entire slab, with a layer of compacted material of minimal thickness placed beneath the slab, adhering to standard construction practices. Beneath this layer of reduced thickness, two additional layers are observed that are thicker than the layers above, reflecting the natural soil characteristics of the area.
4. When analyzing the radargrams near the retaining wall on the south side adjacent to 134th Street, we can observe that the platform's soil foundation structure is disturbed in several areas, and a large number of these alterations coincide with the location of the trees in the outer part. There are noticeable changes in thickness and continuity of the strata and some anomalies that do not go along with the structural frames, probably due to the drying effect caused by the roots of nearby trees. This effect is present from the wall to the axis of the first column, where surface damage is evident in some cases. Likewise, characteristics of affectation can also be seen in the sets of short profiles taken on the surface of affected parking areas.
5. The difference between the subsoil observed in nearby radargrams and the" Weeping Willows" tree section is remarkable. These are areas to stay away from, based on the radargram analysis in the presented affected and unaffected areas.
6. As the profiles move away from the area close to the Weeping Willows, the affectation gradually becomes less until it disappears, the coherence of the strata is clearest.

Acknowledgments

We want to acknowledge the Las Galias Construction Company for their support and help in providing the team of professionals, including geotechnical, structural, and environmental engineers, as well as surveyors, who verified the correlation of these results with other studies the company has regarding this case. We would also like to express our sincere gratitude to the anonymous reviewers for their invaluable suggestions, which greatly enriched and strengthened this work.

References

Alani, A., Bianchini, L., Lantini, L., Tosti, F., Benedetto, A., 2018. Mapping the root system of matured trees using ground penetrating radar. In: 17th International Conference on Ground Penetrating Radar. Rapperswil, Switzerland, pp. 18-21.

Baker, G., Jordan, T., Talley, J., 2007. An introduction to ground penetrating radar. The Geological Society of America, Special Paper 432.

Besson, A., 2010. The spatial and temporal organization of soil water at the field scale as described by electrical resistivity measurements. European Journal of Soil Science, 61 (1): p. 120-132.

Böniger, U., Tronicke, J., 2010. Improving the interpretability of 3D GPR data using target–specific attributes: application to tomb detection. Journal of Archaeological Science. 37(2), 360–367. doi:10.1016/j.jas.2009.09.049.

Daniels, J., Roberts, R., Vendl, M., 1995. Ground penetrating radar for the detection of liquid contaminants. Journal of Applied Geophysics, v. 33, p. 195–207, doi:10.1016/0926-9851(94)00033-K. dGB, 2019. OpendTect user documentation version 6.4.

Dujardin, J., Douillet, G., Bano, M., Kueppers, U., Dingwell, D., 2017. GPR surveys for the characterization of the pyroclastic deposits from the 2006 eruption of Tungurahua volcano, Ecuador. EAGE. 20th European Meeting of Environmental and Engineering Geophysics Athens, Greece, 14-18 September. p. 6.

Finck, F., 2013. Introduction of a ground penetrating radar system for investigations on concrete structures. Otto-Graf-Journal Vol. 14. Sttutgard, Germany , 1–10.

GSSI, 2017. SIR 4000 Manual. Geophysical Survey Systems, Inc.

GSSI, G. S. S., 2013. GSSI Antennas Manual.

Guo, L., Chen, J., Cui, X., Bihang., F., Henry, L., 2013. Application of ground penetrating radar for coarse root detection and quantification: a review. Plant Soil. 362:1–23, DOI 10.1007/s11104-012-1455-5.

Hruska, J., Cermak, J., Sustek, S., 1999. Mapping tree root systems with ground penetrating radar. Tree Physiology 19, pp. 125–130.

Huber, E., Hans, G., 2018. 2018 17th international conference on ground penetrating radar (GPR). In: RGPR — An open-source package to process and visualize GPR data. p. 1-4. doi 10.1109/ICGPR.2018.8441658. ISSN 2474-3844.

Ihaka, R., Gentleman, R., 1996. R: A language for data analysis and graphics. Journal of Computational and Graphical Statistics, vol. 5, pp. 299-314 .

Jol, H., et al. 2009. Ground penetrating radar. Theory and applications. First Edition. Elsevier. ISBN: 978-0-444-53348-7. p. 545.

Jol, H., Bristow, C. S., 2003. Stratigraphic imaging of the navajo sandstone using ground-penetrating radar. The Leading Edge 22(9): 882-887.

Khwanmuang, W., Udphuay, S., 2012. Ground penetrating radar attribute analysis for visualization of subsurface archaeological structures. The Leading Edge, 31(8). pp. 946 - 949. doi:10.1190/tle31080946.1.

Kvamme, K. L., e. a., 2006. New Approaches to the Use and Integration of Multi-Sensor Remote Sensing for Historic Resource Identification and Evaluation. Report submitted to Strategic Environmental Resource Development Program SERDP SI1263, Washington, D.C. p. 395.

Moore, G., Ryder, C., 2015. The use of ground penetrating radar to locate tree roots. Arboriculture & Urban Forestry. 41(5). pp. 245–259.

Neal, A., 2004. Ground-penetrating radar and its use in sedimentology: principles, problems and progress. Earth-Science Reviews, Vol. 66, pp. 261–330.

Ramón, A., Romero, L., Jáuregui, P., 2010. Aplicación de radares en la penetración del suelo (gpr) para el estudio del sistema radicular en un ecosistema dunar costero. Universidad de Pamplona. Revista Ambiental Agua, Aire y Suelo. Vol. I. p. 54-58.

Taner, M., Koehler, F., Sheriff, R., 1979. Complex seismic trace analysis. GEOPHYSICS, 44(6), 1041–106. doi:10.1190/1.1440994 .

Tomecka-Suchoń, S. 2019. Correction to: Ground penetrating radar use in flood prevention. Acta Geophysica. Springer. 67:1679–1691.

White, R., 1991. Properties of instantaneous seismic attributes. The Leading Edge, 10(7), 26–32. doi:10.1190/1.1436827 .

Zhang, X., Derival, M., Albrecht, U., Ampatzidis, Y., 2019. Evaluation of a ground penetrating radar to map the root architecture of hlb-infected citrus trees. Agronomy. 9,354. doi:10.3390/agronomy9070354.